Proceedings of the Thirty-fifth (2025) International Ocean and Polar Engineering Conference **www.isope.org**
Seoul/Goyang, Korea, June 1-6, 2025

ISBN 978-1-880653-74-6; ISSN 1098-6189

Estimation of Hydrodynamic Coefficients of Floating Offshore Structures using the Aggregated Unfitted Finite Element Method

Jan Modderman and Oriol Colomés
Faculty of Civil Engineering and Geosciences, Delft University of Technology
Delft, Zuid-Holland, The Netherlands

ABSTRACT

This work presents a novel application of an Aggregated unfitted Finite Element Method (AgFEM) to solve the linear radiation potential flow problem in the frequency domain to estimate added mass and added damping for floating structures of arbitrary geometry. The flexibility of AgFEM in handling complex geometries makes it a compelling alternative to conventional techniques. The governing equations of the flow problem and the dynamics of the structure are fully coupled. Two case studies are conducted, estimating the loads on a spar and semi-submersible. The results demonstrate that AgFEM captures the general trends of the added mass and damping.

KEY WORDS: Aggregated unfitted Finite Element Method; floating offshore structure; added mass; added damping; linear potential flow; radiation problem.

INTRODUCTION

Fast, accurate, and automated assessments are essential for the safety, performance, and economic viability of offshore renewable energy technologies such as wind and wave converters. Floating structures are crucial in this transition. As demand for offshore energy solutions increases, the design and analysis of floating structures must adapt to complex environments and large-scale deployments. In preliminary design, potential flow theory is typically used for hydrodynamic analysis, assuming incompressible, irrotational flow and neglecting viscous effects. Simplifications like linearized potential flow theory or Airy theory apply under ideal conditions with small wave steepness and basic geometries, enabling analytical methods to estimate hydrodynamic loads and structural responses. However, these methods fail with complex structures or challenging wave conditions.

Numerical methods are essential for addressing arbitrary geometries, nonlinearities, and realistic environmental conditions. The Boundary Element Method (BEM) is popular in offshore engineering for wave-structure interaction problems (Newman and Lee, 2002) because it reduces the problem to the boundary, minimizing unknowns. However, it is limited by high computational demands in large-scale simulations due to dense algebraic systems (Wang et al., 2021a), especially with nonlinear potential flow theory for large or multiple structures. Volume discretization methods like the Finite Element Method (FEM) are more competitive for complex geometries or nonlinear problems due to their flexibility and scalability for large-scale simulations. A key advantage of FEM in wave-structure interactions is its ability to couple fluid and elastic structures, crucial for large, flexible floating platforms (Colomés et al., 2023; Agarwal et al., 2024). Note that structural flexibility is out of the scope of this work.

Floating structures with complex geometrical shapes complicate the meshing process needed for numerical methods. When handling intricate or non-watertight geometry like those represented by the STL file format, creating a mesh can be challenging. This issue underscores the importance of unfitted discretization methods. For these methods, the computational mesh does not conform to the geometry of the domain, allowing for greater flexibility in handling complex geometries without requiring mesh adaptation. The geometric surface intersects or cuts the background mesh to yield a discretization of the domain that conforms to its boundary for integration purposes. One drawback of these methods is that these cut cells can lead to ill-conditioned discretizations; this is known as the cut cell problem. Several methods have been proposed to address the drawbacks of unfitted FEMs, such as the Cut Finite Element Method (CutFEM) (Hansbo et al., 2017), the Shifted Boundary Method (SBM) (Main and Scovazzi, 2018), and the Aggregated unfitted Finite Element Method (AgFEM) (Badia et al., 2018).

In wave-structure interaction analysis, such methods are gaining attention for accurately calculating second-order effects in geometries with sharp features. For example, Wang et al. (2021b) utilizes an Extended FEM (XFEM) approach for 2D hydrodynamic analysis. Similarly, Xu et al. (2023) and Tong et al. (2021), present a high-order immersed boundary method with Finite Difference and Harmonic Polynomial Cell approaches, addressing time-based oscillations in moving domains.

The focus of this work is on the application of AgFEM with potential flow theory and rigid floating structures. AgFEM is employed in this work because the problem of linear potential flow in the frequency domain representation is a purely Neumann-type boundary problem, meaning that we can completely avoid using stability parameters by using AgFEM. This work follows the research line of the usage of embedded methods for floating structures as introduced by Wang et al. (2021b),

although we employ AgFEM instead of XFEM. We focus on the application in 3D, which is a limitation of the aforementioned work. We show that AgFEM can be used to simulate complex geometries using STL files besides simpler geometries represented by level-set functions. Lastly, a notable advantage of a method such as AgFEM is the low manual intervention required to setup the computational mesh.

This article is organized as follows. In the next section, the governing equations of the frequency domain representation, discrete problem formulation, and added mass and damping definitions are introduced. Then, two case studies are conducted, namely the estimation of the added mass and the added damping for both the OC3 Phase IV Hywind spar and the OC4 Phase II DeepCWind semi-submersible. The final section discusses and draws conclusions.

THEORY

Problem Setting

In this work, we consider the case of a floating surface-piercing structure in a free surface-flow problem. We assume the flow to be incompressible, inviscid, and irrotational, and we neglect non-linear terms. For the floating structure, we assume the object to be rigid and can thus apply Newton's second law. The degrees of freedom (DOF) considered for the structure are surge, sway, heave, roll, pitch, and yaw. In figure (Fig. 1) the domain definitions are depicted, which consists of a volume denoted by Ω, a seabed boundary at the bottom Γ_{sb}, the free surface at the top Γ_f, the surrounding wall Γ_w that should correspond to the far-field boundary at infinite length and the structure boundary denoted by Γ. Note that we only consider 3D cases in this work and the domain has a cylindrical shape, hence Γ_w appears on both the left and right sides in figure (Fig. 1).

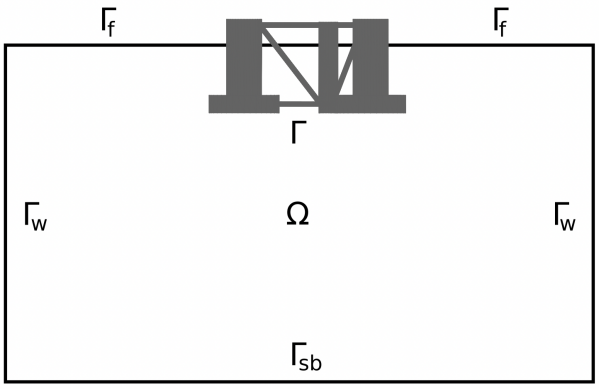

Fig. 1 Overview of domain and boundaries.

Frequency Domain Representation

We assume that the potential field and displacement vector can be decomposed using a Fourier series,

$$\phi(\boldsymbol{x}, t) = \sum_{k=1}^{\infty} \hat{\phi}_k(\boldsymbol{x}) \exp\left(-i\omega_k t + \psi_k\right), \tag{1}$$

$$\boldsymbol{u}(t) = \sum_{k=1}^{\infty} \hat{\boldsymbol{u}}_k \exp\left(-i\omega_k t + \psi_k\right). \tag{2}$$

In this context, $\hat{\phi}_k$ and $\hat{\boldsymbol{u}}_k$ represent complex-valued time-independent amplitudes for each frequency ω_k and phase shift ψ_k. The imaginary unit is denoted by i and k is the index of the Fourier mode. Using the superposition principle of linear systems, we solve separate linear problems for each frequency within the Fourier decomposition. Consequently, for a specific term in the Fourier expansion characterized by frequency ω_k, the problem is expressed as follows:

$$\Delta\hat{\phi}_k = 0 \qquad \text{in} \quad \Omega, \tag{3}$$

$$-\omega_k^2\hat{\phi}_k + g\nabla\hat{\phi}_k \cdot \boldsymbol{n}_{\Gamma_f} = 0 \qquad \text{on} \quad \Gamma_f, \tag{4}$$

$$\nabla\hat{\phi}_k \cdot \boldsymbol{n}_z = 0 \qquad \text{on} \quad \Gamma_{sb}, \tag{5}$$

$$\nabla\hat{\phi}_k \cdot \boldsymbol{n}_{\Gamma_w} - ik\hat{\phi}_k = 0 \qquad \text{on} \quad \Gamma_w, \tag{6}$$

$$\nabla\hat{\phi}_k \cdot \boldsymbol{n}_\Gamma + i\omega_k\hat{\boldsymbol{u}}_k \cdot \boldsymbol{n}_{\Gamma,j} = 0 \qquad \text{on} \quad \Gamma, \tag{7}$$

$$-\omega_k^2\boldsymbol{M}_\rho\hat{\boldsymbol{u}}_k + \int_\Gamma \left(-i\omega\hat{\phi}_k + g\hat{\boldsymbol{u}}_k \cdot \boldsymbol{n}_z\right)\boldsymbol{n}_{\Gamma,j}d\Gamma = \boldsymbol{0} \qquad \text{on} \quad \Gamma. \tag{8}$$

Here, $\hat{\phi}_k$ is the scalar velocity potential, g is the gravitational acceleration constant, the translational normal vectors for each boundary are denoted by $\boldsymbol{n}$ with corresponding boundary subscript, $\boldsymbol{n}_z$ is the normal vector in the vertical direction, $\hat{\boldsymbol{u}}_k$ is the displacement vector of the structure up to 6 DOF, $\boldsymbol{n}_{\Gamma,j}$ is the 6 DOF normal vector on the structure with $\boldsymbol{n}_{\Gamma,j} = \boldsymbol{n}_\Gamma$ for $j = 1, 2, 3$ and $\boldsymbol{n}_{\Gamma,j} = \boldsymbol{r} \times \boldsymbol{n}_\Gamma$ for $j = 4, 5, 6$, and $\boldsymbol{M}_\rho$ is the mass matrix divided by the scalar fluid density $\rho = 1025$ kg/m^3

The wall boundary condition should correspond to a far-field boundary, and therefore we apply a Sommerfeld radiation condition in (6). For ease of notation, we will omit the hat symbol and the subscript k from this point forward, which means $\phi \equiv \hat{\phi}_k$, $\boldsymbol{u} \equiv \hat{\boldsymbol{u}}_k$, and $\omega \equiv \omega_k$.

Discrete Problem Formulation

AgFEM improves matrix conditioning by aggregating degrees of freedom in cut elements to degrees of freedom in interior elements. In order to embed the geometry into the background mesh, we apply the cell cutting algorithms as described by Badia et al. (2018) and Martorell and Badia (2024).

We are required to rewrite the strong formulation in Equations (3)-(8) to a discretized weak formulation stated as:

find $[\phi_h, \boldsymbol{u}_h] \in \mathcal{W}_h \times \mathcal{V}_h$ such that

$$a([\phi_h, \boldsymbol{u}_h], [w_h, \boldsymbol{v}_h]) = b([w_h, \boldsymbol{v}_h]) \qquad \forall w_h, \boldsymbol{v}_h \in \mathcal{W}_h \times \mathcal{V}_h, \tag{9}$$

where $\mathcal{W}_h \doteq H^1(\Omega)$ and $\mathcal{V}_h \doteq \mathbb{C}^{d_j}$ a space of vectorial complex numbers of dimension $d_j = 6$. The bilinear and linear terms are defined as follows:

$$\begin{aligned} a([\phi_h, \boldsymbol{u}_h], [w_h, \boldsymbol{v}_h]) := \\ (\nabla w_h, \nabla\phi_h)_\Omega - \frac{\omega^2}{g}(w_h, \phi_h)_{\Gamma_f} + i\omega\left(w_h, \boldsymbol{u}_h \cdot \boldsymbol{n}_{\Gamma,j}\right)_\Gamma + \\ -i\omega\left(\boldsymbol{v}_h, \phi_h\boldsymbol{n}_{\Gamma,j}\right)_\Gamma - \omega^2\frac{M_\rho}{|\Gamma|}(\boldsymbol{v}_h, \boldsymbol{u}_h)_\Gamma + g\left(\boldsymbol{v}_h, (\boldsymbol{n}_z \cdot \boldsymbol{u}_h)\,\boldsymbol{n}_{\Gamma,j}\right)_\Gamma, \end{aligned} \tag{10}$$

and

$$b([w_h, \boldsymbol{v}_h]) := 0. \tag{11}$$

Here, we use parentheses notation to denote the integral over the domain or boundary denoted by the subscript, that is, $(w_h, \phi_h)_\Omega = \int_\Omega w_h\phi_h d\Omega$ and $(\boldsymbol{v}_h, \boldsymbol{u}_h)_\Gamma = \int_\Gamma \boldsymbol{v}_h \cdot \boldsymbol{u} d\Gamma$. Furthermore, in the second term of Equation (8), it is assumed that the pressure distribution is uniform over the boundary, such that $|\Gamma| := \int_\Gamma d\Gamma$.

Added Mass and Added Damping

The discrete form (9) can be expressed in an equivalent block matrix form as follows:

$$\begin{pmatrix} \mathbb{A}_{w\phi} & \mathbb{A}_{wu} \\ \mathbb{A}_{v\phi} & \mathbb{A}_{vu} + \mathbb{C}_{vu} \end{pmatrix} \begin{pmatrix} \boldsymbol{\Phi} \\ \boldsymbol{U} \end{pmatrix} = \begin{pmatrix} \boldsymbol{F}_{\phi} \\ \boldsymbol{F}_{u} \end{pmatrix}, \tag{12}$$

The algebraic system denoted by (12) can be reduced to a single equation by incorporating the effects of $\boldsymbol{\Phi}$, resulting in

$$\left(\mathbb{A}_{vu} + \mathbb{C}_{vu} - \mathbb{A}_{v\phi}\mathbb{A}_{w\phi}^{-1}\mathbb{A}_{wv}\right)\boldsymbol{U} = \boldsymbol{F}_{u} - \mathbb{A}_{v\phi}\mathbb{A}_{w\phi}^{-1}\boldsymbol{F}_{\phi}. \tag{13}$$

Equation (13) is analogous to the equation of motion for a single-degree-of-freedom spring-mass-damper system. In this context, the term $\mathbb{A}_{vu}$ represents the inertia of the body, $\mathbb{C}_{vu}$ is associated with spring stiffness due to hydrostatic restoring forces, and the expression $\mathbb{A}_{v\phi}\mathbb{A}_{w\phi}^{-1}\mathbb{A}_{wv}$ captures the added inertia and damping caused by the fluid surrounding the object. Consequently, this formulation leads to the equation for the added mass matrix as seen in Equation (14) and the equation for added damping matrix as referenced in Equation (15).

$$\boldsymbol{A} = \frac{Re\left(\mathbb{A}_{v\phi}\mathbb{A}_{w\phi}^{-1}\mathbb{A}_{wv}\right)}{\omega^2} \tag{14}$$

$$\boldsymbol{B} = \frac{Im\left(\mathbb{A}_{v\phi}\mathbb{A}_{w\phi}^{-1}\mathbb{A}_{wv}\right)}{\omega} \tag{15}$$

The added mass and added damping matrices considered in this work are of dimension 6x6. It accounts for six degrees of freedom of the structure: three translational and three rotational. Motions are defined as surge, sway, heave, roll, pitch, and yaw for structural degrees of freedom one to six, respectively. The six diagonal terms of the added mass matrix $\boldsymbol{A}$ represent the fluid-induced inertial force that the body experiences in a direction as a result of the acceleration of the surrounding fluid in that same direction. The off-diagonal terms are the fluid-induced inertial force that the body experiences in one motion direction due to acceleration of the surrounding fluid in a different direction of motion.

The added damping matrix $\boldsymbol{B}$ represents the dissipation of energy due to radiation damping, which arises when the body oscillates and generates waves. This wave radiation carries energy away from the body, leading to a resistive force proportional to velocity. The matrix components are the damping force experienced by the structure in a certain direction of motion associated with the velocity in a particular direction of motion, similarly to the added mass terms.

In Table 1 an overview of the components of the added mass and the added damping matrix relevant to this work is presented. It includes the direction of the force that the structure experiences due to acceleration or velocity in a certain direction of motion for added mass or added damping, respectively.

Table 1 Added mass and added damping matrix components.

Force - motion direction	$\boldsymbol{A}$	Unit	$\boldsymbol{B}$	Unit
surge-surge	A_{11}	kg	B_{11}	kg/s
sway-sway	A_{22}	kg	B_{22}	kg/s
heave-heave	A_{33}	kg	B_{33}	kg/s
roll-roll	A_{44}	kg·m^2	B_{44}	kg·m^2/s
pitch-pitch	A_{55}	kg·m^2	B_{55}	kg·m^2/s
yaw-yaw	A_{66}	kg·m^2	B_{66}	kg·m^2/s
surge-pitch	A_{15}	kg·m	B_{15}	kg·m/s
sway-roll	A_{24}	kg·m	B_{24}	kg·m/s

CASE STUDY

We verify the code by comparing the added mass and added damping with the reference added mass and added damping of the OC3 Phase IV Hywind spar floating offshore wind turbine (FOWT) (Jonkman, 2010) and of the OC4 Phase II DeepCWind semi-submersible FOWT (Robertson et al., 2014). The OC3 and OC4 projects are international benchmarking efforts aimed at verifying and validating numerical models for offshore wind turbines through code-to-code comparisons. These projects established standardized validation methodologies that provide a reliable basis for assessing the accuracy of offshore wind turbine simulations. The reference data from the aforementioned works were generated using the WAMIT software package. WAMIT utilizes a 3D BEM in the frequency domain to solve the linearized potential flow equations that govern hydrodynamic radiation for wave interactions with offshore structures.

Although a comparison between the meshing process of a BEM and a FEM can never be fair, we would like to highlight that the meshing process for the simulation for the reference data requires manual refinement to mitigate irregular frequency effects (Jonkman, 2010; Robertson et al., 2014). In contrast, an AgFEM approach requires only the generation of a background mesh.

Software

The software packages used to generate results for this work are *Gridap.jl*, an open-source Finite Element toolbox with sub-packages *GridapEmbedded.jl* and *STLCutters.jl* for the embedding of the structure into the background mesh. The open-source meshing software *GMSH* is used for the generation of background meshes. These software packages are coupled using the sub-package *GridapGmsh.jl*

Geometrical Representation of Hywind and DeepCWind

The OC3 Phase IV spar has a relatively simple geometry, as it consists of two cylinders of different diameters connected via a tapered cylinder. The geometrical representation of the OC4 Phase II DeepCWind semi-submersible consists of four vertical cylindrical columns connected via horizontal and diagonal braces. The three outer columns have wider base columns attached at the bottom. In figure (Fig. 2) the geometry of the OC3 Hywind spar is depicted on the left, and on the right the geometry of the OC4 DeepCWind semi-submersible is depicted.

Computational Domain

The computational domain is setup using the data in Table 2 in which an overview of the relevant domain parameters is shown for each case study. The water depths are selected from both respective reference papers. The characteristic length is chosen to be equal to the largest diameter of the largest component for each of the structures. For OC3, this is the bottom cylindrical section, and for OC4 this corresponds to the diameter of one of the bottom cylindrical sections of the three outer cylinders. From the work by Wang et al. (2021b) we consider the longest wave $\lambda_{\max}$ in this work to be restricted by the nondimensional wave number $\omega^2 D_c/g = 0.1$ with characteristic length D_c. The minimum wavelength $\lambda_{\min}$ is derived from the maximum angular frequency considered in the reference data.

The background mesh should be able to capture the smallest wavelengths at the free surface, whilst the domain radius is limited by the maximum wavelength. Additionally, in the reference data a panel size of 2 m is used on the structure, which is also used in this work. For AgFEM this might be insufficient as the reference data applied enhancements near the logarithmic singularities (Jonkman, 2010; Robertson et al., 2014) allowing for larger panel sizes close to sharp features in the geometry. Given these requirements, a background mesh is created with a minimum characteristic element length $h_{e,\min} = 0.37$ m and a maximum characteristic

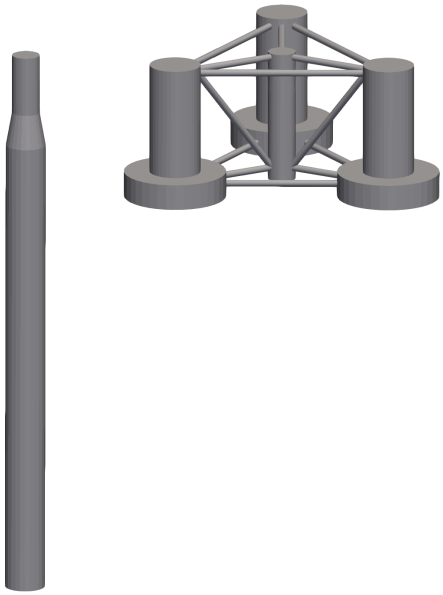

Fig. 2 Geometrical representation of the Hywind spar (left) and the DeepCWind semi-submersible (right).

element length $h_{e,\max}$ = 59.43 m. The background mesh for the OC3 case study is shown in figure (Fig. 3). For the OC4 case study, a similar cylindrical computational domain and background mesh is constructed given the required horizontal domain radius. Note that the requirement on the horizontal domain radius could be relaxed, but that will negatively impact the results for the lower frequency range.

Table 2 Dimensions and relevant parameters for the case study

Study:	OC3	OC4
Water depth: d [m]	320.0	200.0
Characteristic length: D_c [m]	9.4	24.0
Minimum wavelength: $\lambda_{\min}$ [m]	2.5	2.5
Maximum wavelength: $\lambda_{\max}$ [m]	590.6	1507.9
Horizontal domain radius: R_x [m]	600.0	1500.0

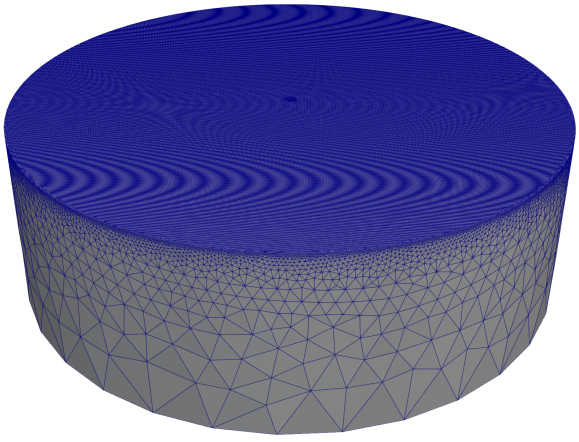

Fig. 3 Background mesh for the OC3 case study.

OC3 Phase IV Hywind Spar

The OC3 Hywind is a spar-type floater, which means that it is expected that the surge and sway forces and the rolling and pitching moments dominate with respect to the heave and yaw. The added mass and added damping terms in and around the horizontal plane, i.e. those coefficients denoted by subscripts 11 and 22, and 44 and 55, are identical due to the geometrical symmetry of the structure.

In figures (Figs. 4~5) the added mass and added damping of the OC3 spar are depicted, respectively. It appears that the added mass slightly underestimates the reported values from Jonkman (2010). The added damping matches well, and for higher frequency values we report oscillations for surge-surge B_{11} and sway-sway B_{22}. These oscillations might be due to elements not fully capturing the wavelength at those higher frequencies.

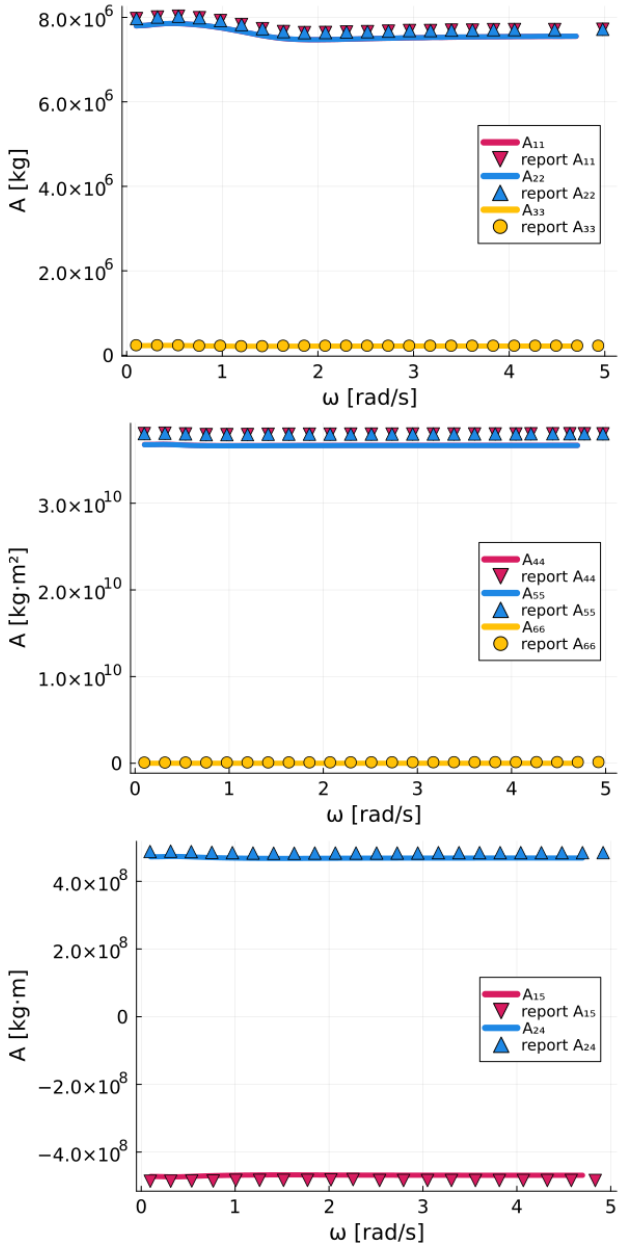

Fig. 4 Added mass matrix terms of OC3 for the six diagonal terms A_{11} to A_{66} and the off-diagonal A_{15} and A_{24}.

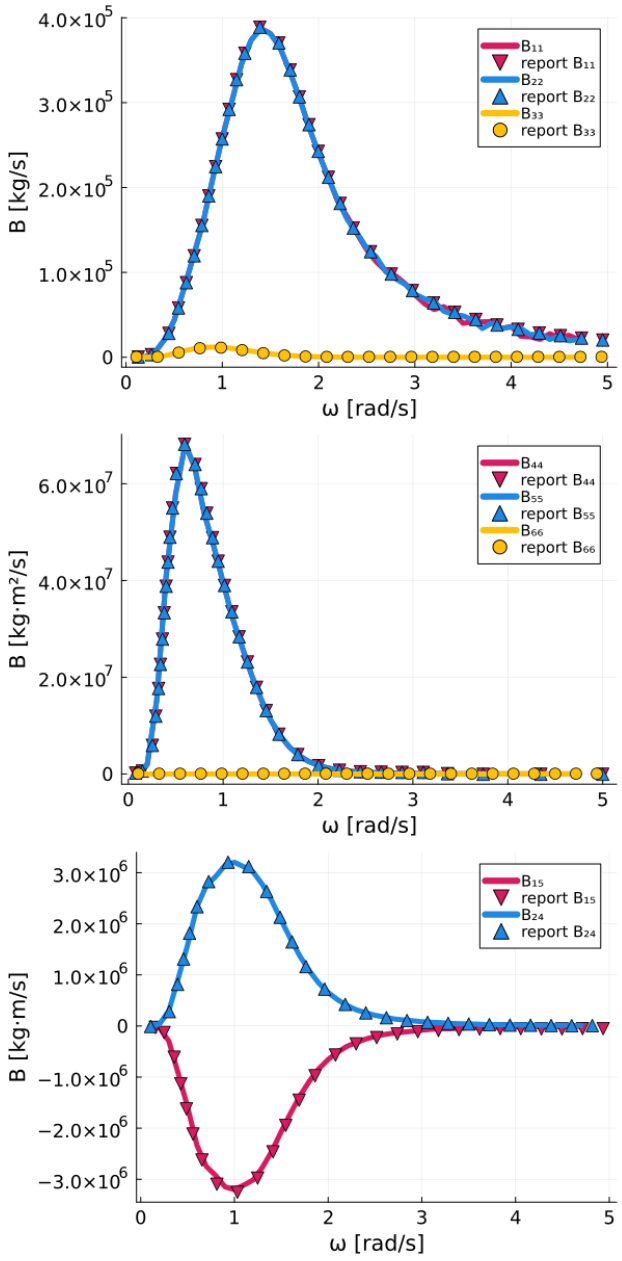

Fig. 5 Added damping matrix terms of OC3 for the six diagonal terms B_{11} to B_{66} and the off-diagonal B_{15} and B_{24}.

OC4 Phase II DeepCWind Semi-submersible

The OC4 DeepCwind is a semi-submersible type floater, meaning the heave force and yaw moment are significantly larger than the forces in and moments around the horizontal. In figure (Fig. 6) the added mass over the angular frequency is plotted for the diagonal terms of the added mass matrix and for the off-diagonal terms: surge-pitch A_{15} and sway-roll A_{24}. The reported values from Robertson et al. (2014) are depicted using marker symbols. It is clear that the current method underestimates the added mass forces and moments, especially for heave-heave A_{33}, roll-roll A_{44} and pitch-pitch A_{55} the discrepancy is significant. However, it correctly captures the behavior over the frequency as the peaks and troughs match the reference data. Indicating that the equations are solved correctly. Furthermore, due to geometrical symmetries, the terms surge-surge A_{11} and sway-sway A_{22}, and roll-roll A_{44} and pitch-pitch A_{55} are expected to be identical, as confirmed by the AgFEM model. The differences between the AgFEM model and the reference values might be a matter of mesh resolution. Especially close to the lower base columns, a highly refined mesh is required.

In figure (Fig. 7) the added damping is depicted in the same terms. These results match well with the values reported by Robertson et al. (2014), matching both the amplitude and phase. However, for the higher frequency range there appear more oscillations in the AgFEM model. This is likely to be due to the mesh resolution being too coarse for the small wavelengths located in this frequency range.

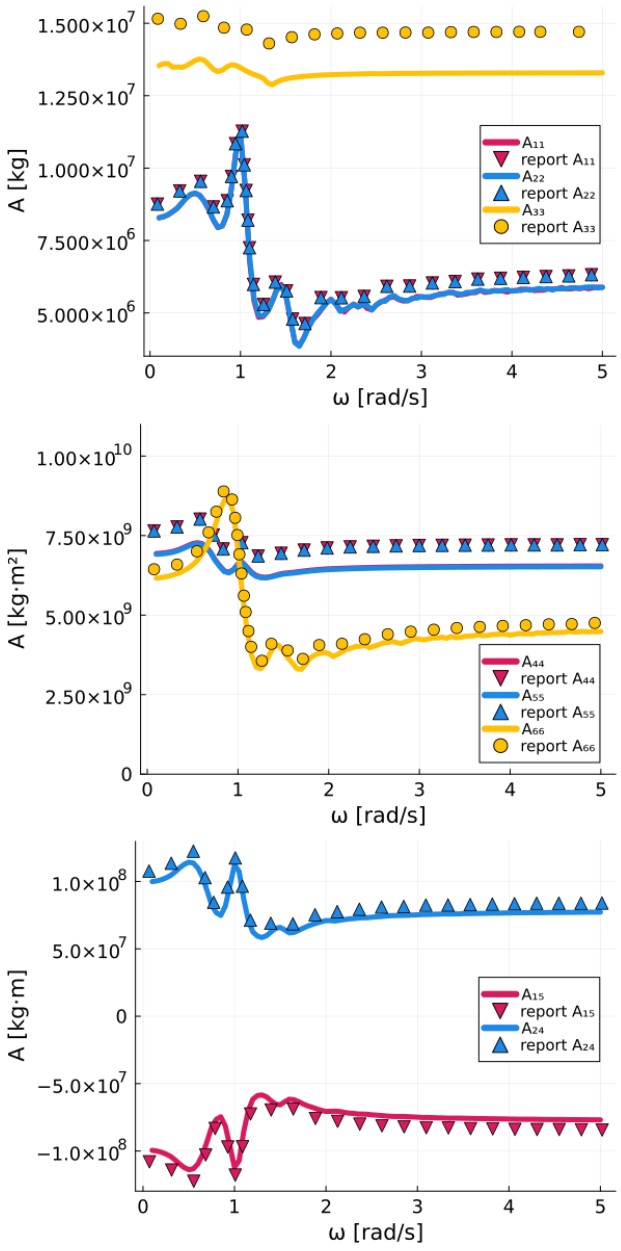

Fig. 6 Added mass matrix terms of OC4 for the six diagonal terms A_{11} to A_{66} and the off-diagonal A_{15} and A_{24}.

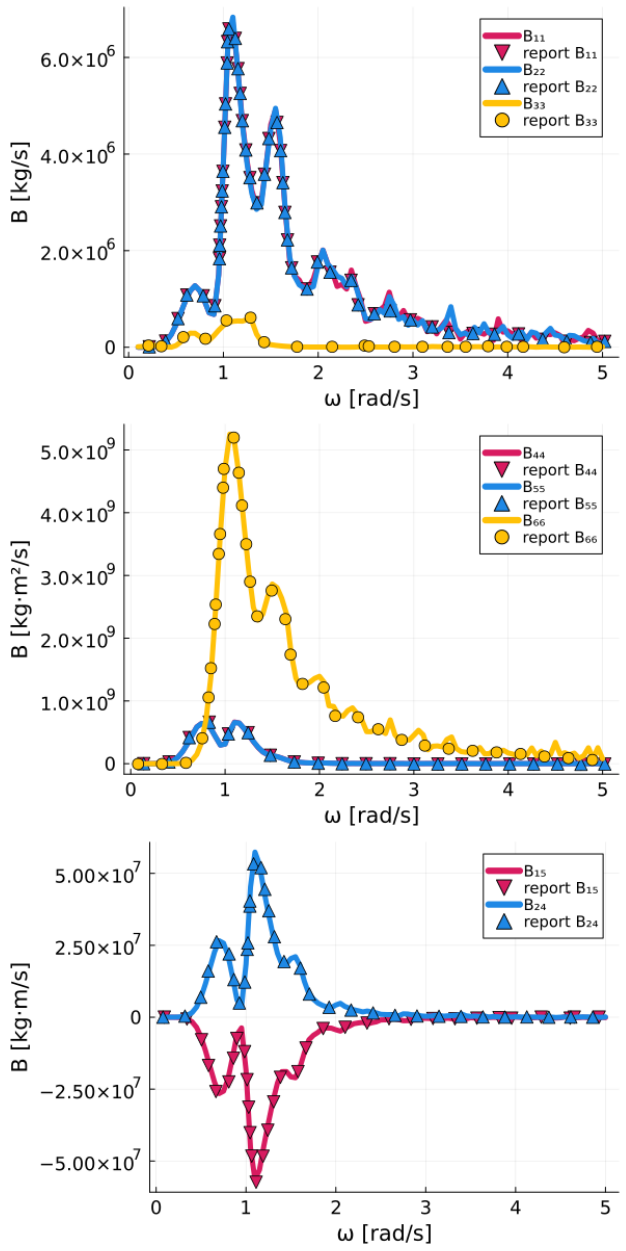

Fig. 7 Added damping matrix terms of OC4 for the six diagonal terms B_{11} to $B_{66}$and the off-diagonal B_{15} and B_{24}.

CONCLUSIONS AND DISCUSSION

In this work, we presented a novel application of the Aggregated unfitted Finite Element Model, which solves for a linear potential flow frequency domain representation to estimate added mass and added damping for floating structures of arbitrary geometry. The proposed method does not require manual intervention in the meshing procedure after a non-conforming background mesh has been generated. The results appear promising, as the general trends of added mass and added damping are recovered for both case studies.

However, more conclusive research should be conducted on the required dimensions of the domain and the minimum mesh refinement required to make this tool more competitive. Domain sizes can become large when the maximum wavelength is taken into account. In addition, the minimum wavelength indicates the element size at the free surface, and this combination requires a large number of elements in the mesh. This allows for further research and applications using a symmetry condition or numerical damping zones or the addition of a Perfectly Matched Layer (PML) to reduce domain size. Arbitrary mesh refinement should be coupled to the existing model using a forest of octrees based on cut elements for optimal refinement. Finally, to highlight this model's capabilities, an extension to multi-body is straightforward and will be studied in future works.

REFERENCES

Agarwal, S and Colomés, O and Metrikine, A. (2024). "Dynamic analysis of viscoelastic floating membranes using monolithic Finite Element method", *Journal of Fluids and Structures* Vol. 129, pp. 104167.

Badia, S, Verdugo, F and Martín, A. (2018). "The aggregated unfitted finite element method for elliptic problems", *Computer Methods in Applied Mechanics and Engineering* Vol. 336, pp. 533-553.

Colomés, O and Verdugo, F and Akkerman, I. (2023). "A monolithic finite element formulation for the hydroelastic analysis of very large floating structures ", *International Journal for Numerical Methods in Engineering* Vol. 124, No. 3, pp. 714–751.

Hansbo, P, Larson, M and Larsson, K. (2017). "Cut finite element methods for linear elasticity problems", *Geometrically Unfitted Finite Element Methods and Applications: Proceedings of the UCL Workshop 2016* pp. 25-63.

Jonkman, J. (2010). "Definition of the Floating System for Phase IV of OC3", *NREL Technical Report* NREL/TP-500-47535.

Main, A and Scovazzi, G. (2018). "The shifted boundary method for embedded domain computations. Part I: Poisson and Stokes problems", *Journal of Computational Physics* Vol. 372, pp. 972-995.

Martorell, P and Badia, S. (2024). "High order unfitted finite element discretizations for explicit boundary representations", *Journal of Computational Physics* Vol. 511, pp. 113127.

Newman, J and Lee, C-H. (2002). "Boundary-element methods in offshore structure analysis", *Journal of Offshore Mechanics and Arctic Engineering*, Vol. 124, No. 2 pp. 81-89.

Robertson, A, Jonkman, J, Masciola, M, Song, H, Goupee, A, Coulling, A and Luan, C. (2014). "Definition of the semi-submersible floating system for phase II of OC4", *NREL Technical Report* NREL/TP-5000-60601.

Tong, C, Shao, Y, Bingham, H and Hanssen, F-C. (2021). "An adaptive harmonic polynomial cell method with immersed boundaries: Accuracy, stability, and applications", *International Journal for Numerical Methods in Engineering* Vol. 122, No. 12, pp. 2945–2980.

Wang, W, Pákozdi, C, Kamath, A and Bihs, H. (2021a). "A fully nonlinear potential flow wave modelling procedure for simulations of offshore sea states with various wave breaking scenarios", *Applied Ocean Research* Vol. 117, pp. 102898.

Wang, Y, Shao, Y, Chen, J and Liang, H. (2021b). "Accurate and efficient hydrodynamic analysis of structures with sharp edges by the Extended Finite Element Method (XFEM): 2D studies", *Applied Ocean Research* Vol. 117, pp. 102893.

Xu, Y, Bingham, H and Shao, Y. (2023). "A high-order finite difference method with immersed-boundary treatment for fully-nonlinear wave–structure interaction", *Applied Ocean Research* Vol. 134, pp. 103535.